CFD Analysis on Propeller at Varying Propeller Disc Angle and Advance Ratio

Leong Chee Hang[1], Nur Athirah Nadwa Rosli[1], Mastura Ab Wahid[1,*], Norazila Othman[1], Shabudin Mat[1], Mohd Zarhamdy Md Zain[2]

[1] Department of Aeronatical, Automotive and Offshore Engineering, Faculty of Mechanical Engineering, Universiti Teknologi Malaysia, 81310 Skudai, Johor, Malaysia
[2] Department of Applied Mechanics and Design Engineering, Faculty of Mechanical Engineering, Universiti Teknologi Malaysia, 81310 Skudai, Johor, Malaysia

ARTICLE INFO	ABSTRACT
	The purpose of this study is to see the feasibility of using Computational Fluid Dynamic (CFD) analysis over wind tunnel testing for propeller performance measurement. Computational Fluid Dynamic (CFD) analysis is conducted on APC 6X4E propeller and 9X6E propeller at propeller disc angle, α of 0°, 30°, 60°, and 90° using commercially available software ANSYS FLUENT at advance ratio ranging from 0 to 0.88 and angular velocity ranging from 1000rpm to 8000rpm. CFD analysis was also performed for different advance ratio at different rotational speed of 4000rpm and 8000rpm. Multiple Reference Frame model is used to simulate the rotating propeller in a flowing airstream by constructing a rotating and static domain around the propeller. The non-zero propeller disc angle is achieved by changing the inlet direction of the static domain. The SST k-ω turbulence model is used, and tetrahedral mesh is constructed. The propeller thrust and torque obtained from the CFD simulation is used to calculate the aerodynamic characteristics of the propellers. The thrust coefficient, torque coefficient and propeller efficiency obtained for both propellers follow the trend of the wind tunnel testing. The results obtained from the CFD simulation matches with the results trend obtained by another researcher performing wind tunnel analysis, where the thrust coefficient decreases with increasing advance ratio at propeller disc angle less than 60° and increases with increasing advance ratio at propeller disc angle more than 70°. The error produce for thrust estimation is lower than 12% for both 6x4E and 9x6E propellers. The error for torque and efficiency estimation is between 15-30% and 12% respectively. In conclusion, CFD simulation can predict the aerodynamic characteristics of Low Reynolds Number propeller at different propeller disc angle.

1. Introduction

Before the rise of quadrotor and multirotor UAV's, past research on Low Reynolds Number propeller were mainly focused on the aerodynamic characteristics of the propeller when it is parallel to the free stream or the propeller disc angle of attack, α_p = 0°. Due to the unique propeller

---

configuration for quadrotor and multirotor UAV's where the propeller is perpendicular to the freestream and the maneuver by tilting the propeller, the aerodynamic performance of the propeller at different propeller disc angle of attack is essential for the performance of the UAV's.

While majority of research on aerodynamic characteristics of propellers at different propeller disc angle of attack focuses on large propellers, there are a few research on Low Reynolds Number propeller at different propeller disc angle using wind tunnel testing method. Serrano *et al.,* [1] conducted an investigation to determine the aerodynamic performance of four propeller with diameter 12-inch with propeller disc angle of attack ranging from 0° to 90° and advance ratio ranging from 0 to 0.55 [1]. Based on the researches, the propeller thrust increased with as the propeller disc angle of attack increased, while the power consumption shows low sensitivity to the changes of the propeller disc angle of attack [1]. Majority of the research on aerodynamic characteristics of Low Reynolds Number propellers are using the wind tunnel testing method and there is lack of research on that topic using CFD analysis. Therefore, this study aims to validate the use of CFD analysis in obtaining the aerodynamic characteristics of Low Reynolds Number propeller at different propeller disc angle of attack. Study from Mohamed *et al.,* [15] researched on slotted airfoil. Based on the study, introducing slotted airfoil for low Reynolds number propeller reduces the efficiency of the propeller.

Reynolds-averaged approach is used to solve the turbulence flow simulation as it is robust, economical, and relatively accurate. This approach is used by many commercially available software such as ANSYS Fluent. In Reynolds-average approach, selection of turbulence model is an important and it influence the simulation results accuracy. The selection of turbulence model depends on the type of simulation. For turbomachinery, the common turbulence model used are Spalart-Allmaras (S-A) model, and k-ε model. For example, Seeni *et al.,* [2] conducted an CFD simulation on APC10x7SF propeller using Spalart-Allmaras (S-A) turbulence model and validated the result by comparing it to the experimental result. This study will aim to conduct CFD simulation on propeller at varying propeller disc angle and obtain the propeller aerodynamic performance.

2. Methodology
2.1 K-ω Turbulence Model

The SST k-ω is proposed by Menter [7] by combining the standard k-ε model and standard k-ω. This model uses a cross-diffusion term in the transport equation for specific dissipation rate, ω. This enables the model to predict the flow at near-wall location using the k-ω turbulence model and predict the flow far away from wall using standard k-ε turbulence model [3]. The transport equation for turbulent kinetic energy, κ is represented by

$$\frac{\partial \kappa}{\partial t} + \frac{\partial}{\partial x_i}(\bar{u}_i \kappa) = \frac{\partial}{\partial x_i}\left(\nu + \frac{\nu_T}{\sigma_k}\right)\frac{\partial \kappa}{\partial x_i} + \frac{\bar{\tau}_{ij}^R}{\rho}\frac{\partial \bar{u}_i}{\partial x_j} - \varepsilon \tag{1}$$

where $\bar{\tau}_{ij}^R$ is the Reynolds stress tensor, ρ is the density, and σ_k is the diffusion Prandtl number for turbulent kinetic energy. The transport equation for turbulence energy dissipation rate, ε is represented by

$$\frac{\partial \varepsilon}{\partial t} + \frac{\partial}{\partial x_i}(\bar{u}_i \varepsilon) = \frac{\partial}{\partial x_i}\left(\nu + \frac{\nu_T}{\sigma_\varepsilon}\right)\frac{\partial \varepsilon}{\partial x_i} + C_{\varepsilon 1}\frac{\varepsilon}{\kappa}\frac{\bar{\tau}_{ij}^R}{\rho}\frac{\partial \bar{u}_i}{\partial x_j} - C_{\varepsilon 2}\frac{\varepsilon^2}{\kappa} \tag{2}$$

where $C_{\varepsilon 1}$ = 1.44, $C_{\varepsilon 2}$ = 1.92, σ_ε is the diffusion Prandtl number for isotropic turbulence energy dissipation rate and is equal to 1.3 [4]. Meanwhile the eddy viscosity for k-ε model is expressed as

$$v_T = C_\mu \frac{\kappa^2}{\varepsilon} \tag{3}$$

where C_μ = 0.09.

The transport equation for specific dissipation rate, ω is expressed as

$$\frac{\partial \rho \omega}{\partial t} + \frac{\partial}{\partial x_i}(\rho \omega u_i) = \frac{\partial}{\partial x_j}\left[(\mu + \sigma_\omega \mu_T)\frac{\partial \omega}{\partial x_j}\right] + \frac{\gamma}{v_T}P - \beta \rho \omega^2 + 2(1 - F_1)\frac{\rho \sigma_{\omega 2}}{\omega}\frac{\partial \kappa}{\partial x_j}\frac{\partial \omega}{\partial x_j} \tag{4}$$

where the turbulent eddy viscosity is represented by

$$\mu_T = \frac{\rho a_1 \kappa}{\max(a_1 \omega, \Omega F_2)} \tag{5}$$

The function F_1 and F_2 are given by

$$F_1 = \tanh(arg_1^4) \tag{6}$$

$$arg_1 = min\left[\left(\frac{\sqrt{\kappa}}{\beta^* \omega d}, \frac{500v}{d^2 \omega}\right), \frac{4\rho \sigma_{\omega 2}\kappa}{CD_{\kappa\omega}d^2}\right] \tag{7}$$

$$CD_{\kappa\omega} = \max\left(2\rho\sigma_{w2}\frac{1}{\omega}\frac{\partial \kappa}{\partial x_j}\frac{\partial \omega}{\partial x_j}, 10^{-20}\right) \tag{8}$$

$$F_2 = \tanh(arg_2^2) \tag{9}$$

$$arg_2 = \max\left(2\frac{\sqrt{\kappa}}{\beta^* \omega d}, \frac{500v}{d^2 \omega}\right) \tag{10}$$

The constants used is a_1 = 0.31, κ = 0.41, β^* = 0.09 and $\sigma_{\omega 2}$ = 0.856. The SST k-ω turbulence model is a blend of k-ε model and k-ω model. This eliminate the weakness for k-ε model which is inaccurate prediction at near wall location and the weakness of k-ω model which is too sensitive to the freestream turbulence condition. This model gives better result with flow that involves separation of flow. However, the weakness of this model is it requires higher computation power due to the additional function F_1 and F_2.

2.2 Domain Modelling

Two propellers with different diameter and pitch which is APC 6X4E propeller and APC 9X6E propeller are purchased and to be measured physically. The aerofoil of the propeller blade consists of low Reynolds number Eppler E63 aerofoil blended with a Clark-Y similar aerofoil at the tip of the propeller blade. Figure 1 shows the chord and twist distribution for the propellers.
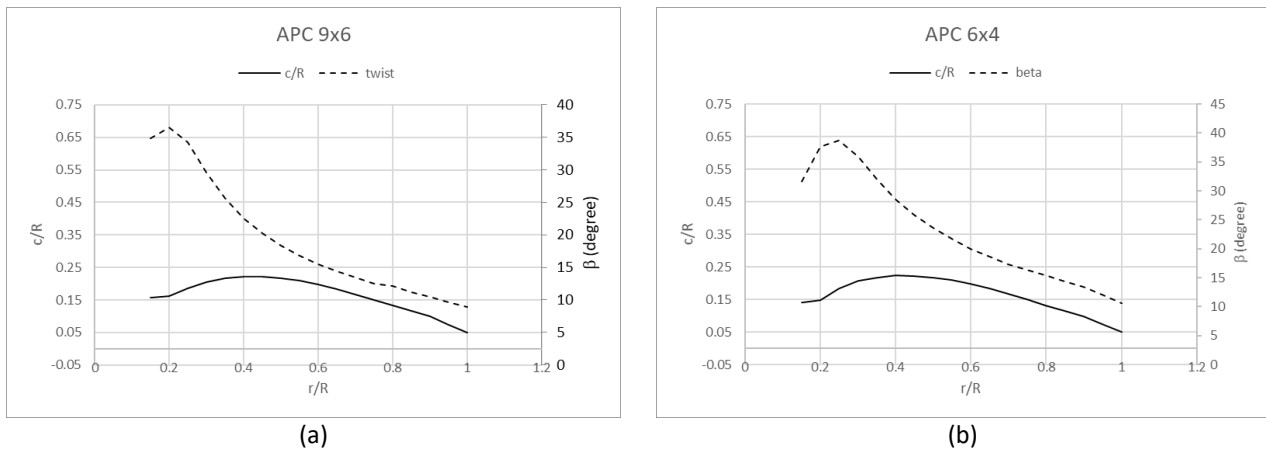
Fig. 1. (a) Top and (b) side view sketch of 9x6E and 6X4E propeller

The multiple reference frame (MRF) model approach is used. This approach is widely used for the analysis for turbomachinery that consist of rotating part and a fixed part [2,5,6]. To imitate the flow in wind tunnel testing, the domain of the flow is separated into stationary domain and rotating domain. The rotating domain is a small cylinder that enclose the propeller with the boundary close to the propeller while the stationary domain is represented by a larger cylinder that enclose the rotating domain and propeller with the boundary further away from the propeller. For CFD analysis on the propellers at different propeller disc angle, the size of the static domain is remained constant while the direction of the inlet is changed to achieve the effect of desired propeller disc angle. Figure 2 below shows the full domain of the model used for simulation at non-zero propeller disc angle.
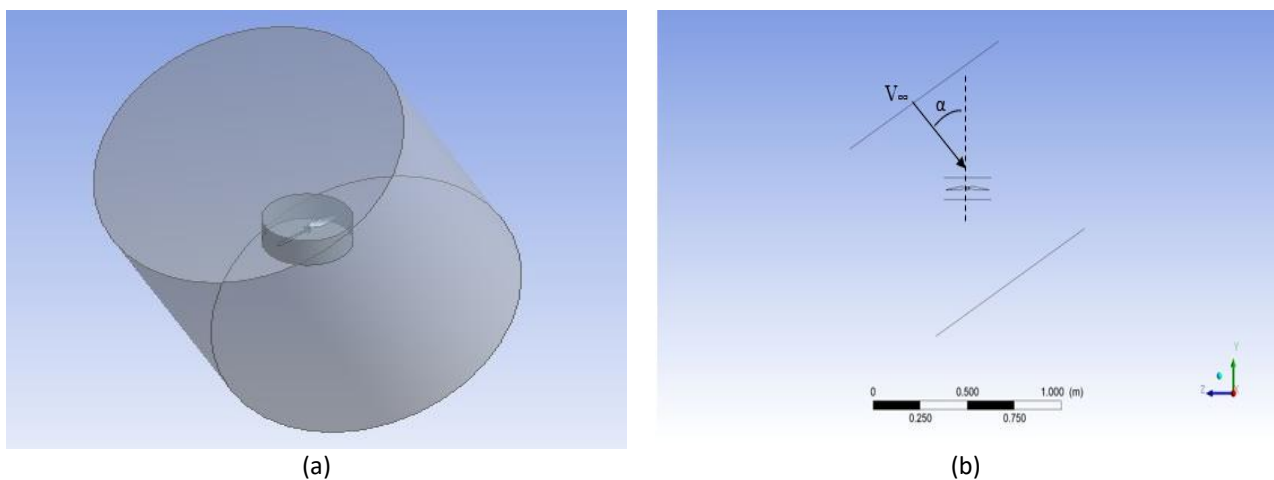

Fig. 2. (a) Isometric view and (b) Top View of the CFD domain for non-zero propeller disc angle

2.2 Mesh Generation

The meshing for the model stationary domain, rotating domain and propeller is generated using the built-in mesh tool in ANSYS FLUENT. Tetrahedral mesh is constructed with capture proximity and capture curvature built in settings in ANSYS FLUENT. The element size for the mesh at the propeller and rotating region are finer compared to the element size of the static region mesh as this project intend to focus on the flow around the propeller to obtain the lift and drag coefficient of the propeller. To eliminate the mesh discretization error, mesh convergence test is conducted by recording the thrust of the propeller at decreasing mesh size until convergence of result is obtained. Then, the element size is where the result converges is chosen. The meshing of the propeller is shown

in Figure 3 where the element size for the propeller is smaller and the size increase moving further away from the propeller. Study from Seeni *et al.,* [2] has come up with a fitting method to overcome grid independent issues and from the result, the range of the error is about 3-70% of error as the advance ratio increase from 0.192 to 0.799 respectively.
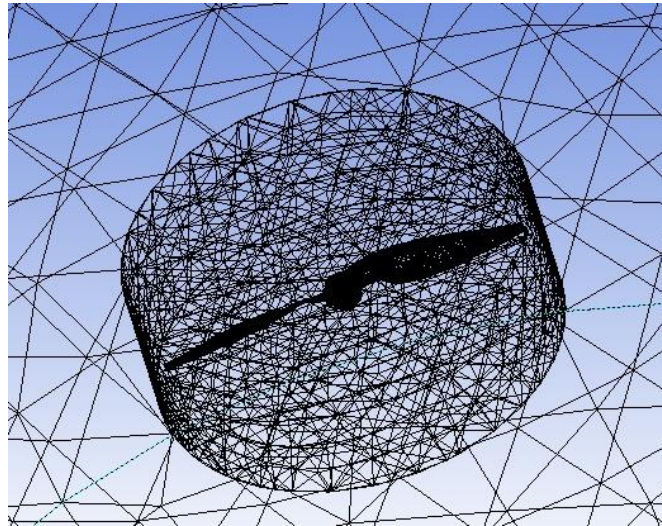

Fig. 3. Meshing of the propeller and its domain

Mesh convergence test is conducted by recording the thrust of the propeller at decreasing mesh size until convergence of result is obtained. 4 different meshes consisting of tetrahedral meshes is constructed to test the convergence of the data. The first 3 mesh constructed is the default meshing using ANSYS Fluent with coarse, mid, and fine meshing while the fourth meshing constructed is fine mesh with capture curvature and proximity settings on. The information of the mesh generated is shown in Table 1. The mesh convergence test is tested by running simulation on the 9x6E APC propeller model at 1000rpm and 0 ms^{-1} inlet velocity using standard k-ε model. The propeller thrust results are plotted against the number of mesh element and compared to the manufacturer data. The mesh convergence test in Figure 4 shows that the result converges as the number of mesh element increases and the simulation result for the highest number of mesh elements is closest to the experimental data. This mesh is chosen as the final mesh as the result converges and further increase in element number will only cost more computation power and low effect on the accuracy of the analysis.

Table 1
Number of mesh elements for different mesh configuration

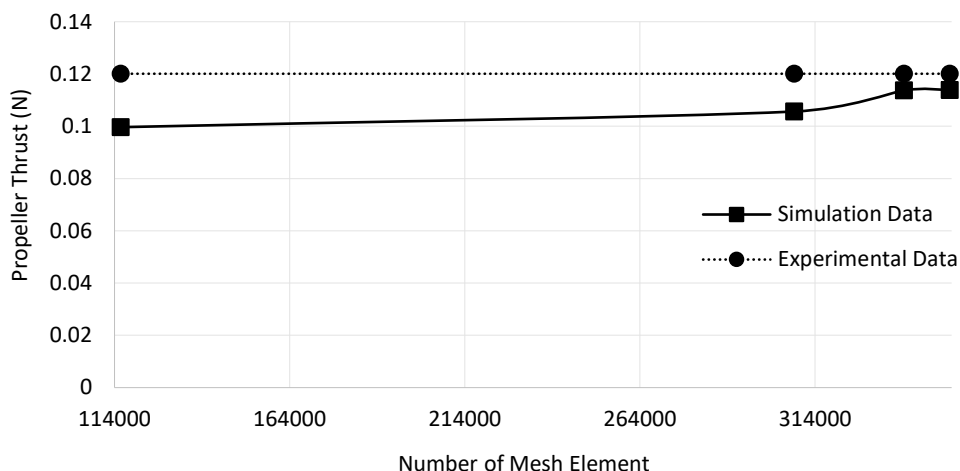| Configuration	Mesh Element
Coarse	115729
Medium	308082
Fine	339360
Fine mesh with capture curvature and proximity settings selected	352496

Fig. 4. Mesh Convergence Test

2.2 Selection of Turbulence Model

Selection of turbulence model is an important step in setting up a CFD simulation. Static thrust CFD analysis is conducted at zero propeller disc angle with angular velocity ranging from 1000rpm to 8000rpm using different turbulence model. The CFD simulation result is then compared with the manufacturer data to determine the most suitable turbulence data that match the manufacturer and UIUC experiment data [8,16] closely as shown in Table 2. For both 6X4E propeller and 9X6E propeller, SST k-ω model shows more accurate result compared to standard k-ε model, Spalart-Allmaras (S-A) model, and standard k-ω model as shown in Figure 5 and Figure 6. Therefore, the SST k-ω model is used for this study.
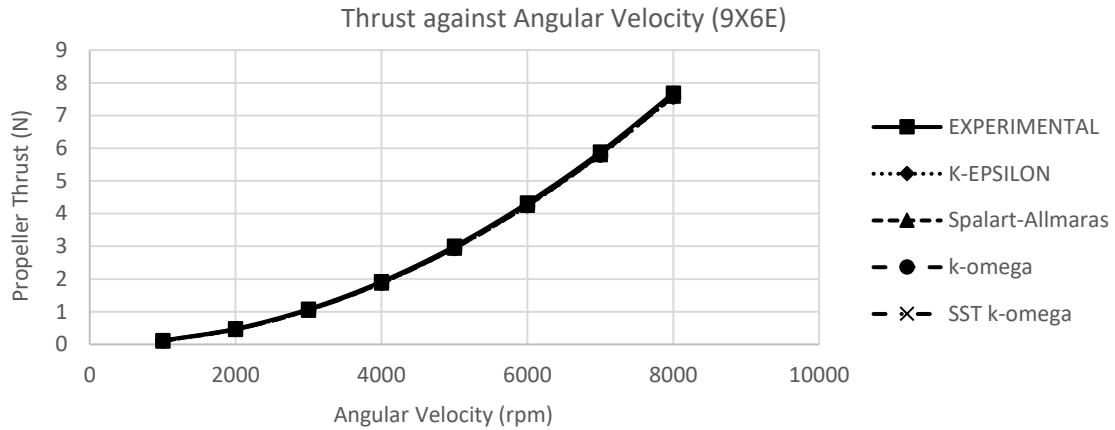

(a)

(b)
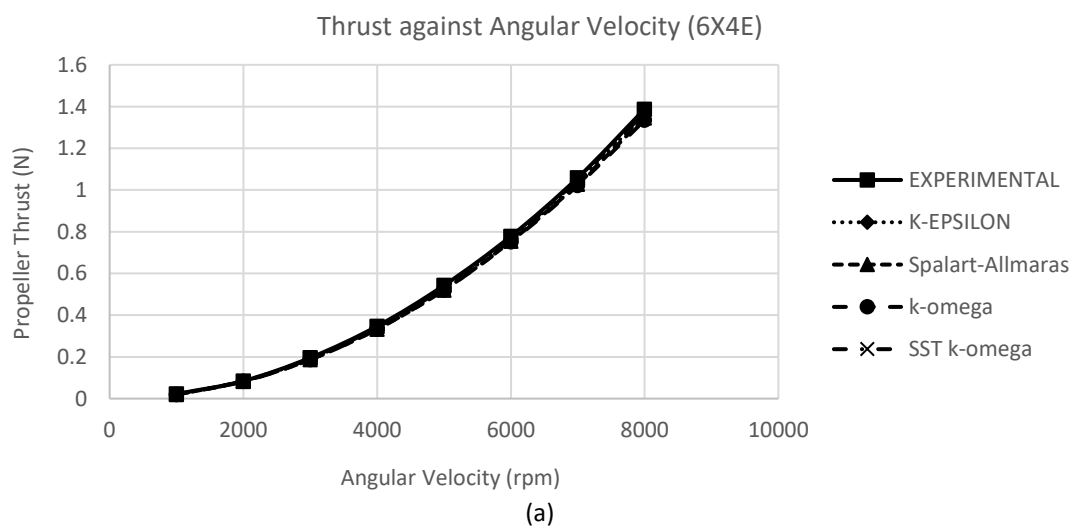
Fig. 5. Propeller thrust against propeller angular velocity curve for (a) 6X4E and (b) 9x6E propeller
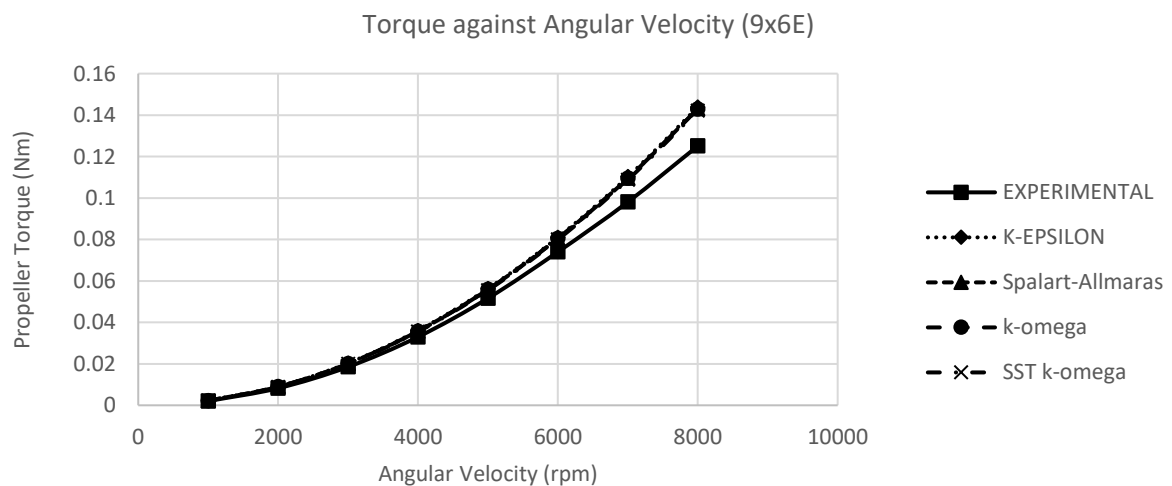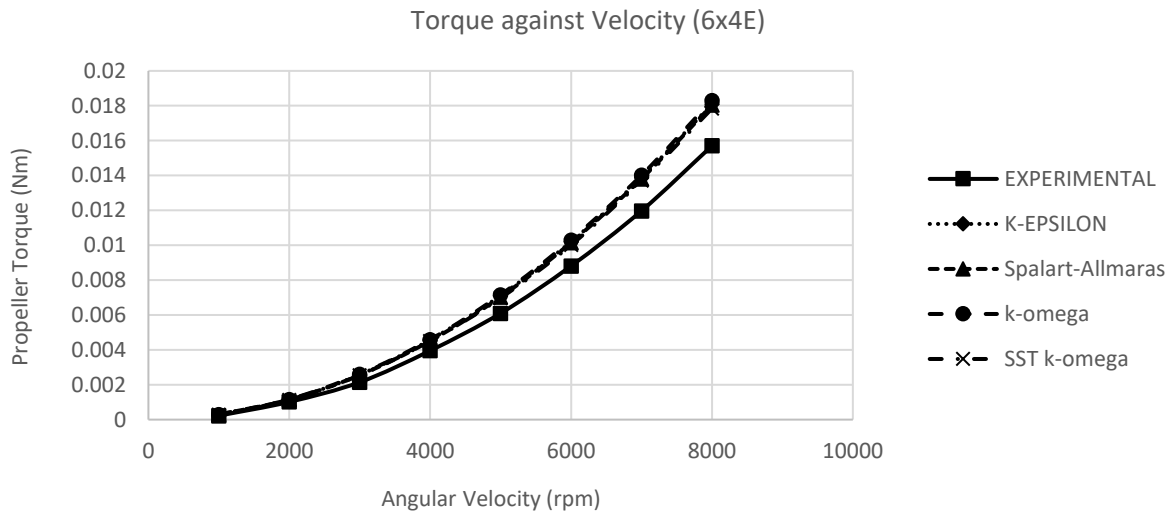

(a)

(b)

Fig. 6. Propeller torque against propeller angular velocity curve for (a) 6X4E and (b) 9x6E propeller

Table 2
Percentage error of different turbulence model simulation result compared to manufacturer experimental data

Turbulence Model	Percentage Error (%)			
	6x4E		9x6E	
	Propeller Thrust	Propeller Torque	Propeller Thrust	Propeller Torque
Standard k-ε model	2.41	17.63	2.69	10.73
Spalart-Allmaras model	4.34	16.68	2.76	9.68
Standard k-ω model	4.62	18.60	3.02	9.78
SST k-ω model	2.54	15.98	2.50	9.03

3. Results

3.1 CFD Simulation of Propeller at Different Advance Ratio

To further validate the use of CFD simulation in determining the aerodynamic characteristics of the Low Reynolds Number propeller. The thrust coefficient, torque coefficient and propeller efficiency of the 9X6E and 6X4E propellers are obtained through CFD simulation and compared with the experimental data. The advance ratio used ranges from 0 to 0.88 while the angular velocity ranges from 4000rpm and 8000rpm. The figures show that thrust coefficient and torque coefficient decreases with the increasing advance ratio for both propellers. For the propeller efficiency, the propeller efficiency increases with the increasing advance ratio and then decreases with the increasing advance ratio at advance ratio ≥ 0.6. The simulation is conducted for 4000rpm and 8000rpm to test the consistency of the CFD simulation at different angular velocity.

Based on the result of CFD simulation, the coefficient of thrust, C_T and C_Q at the same advance ratio result show consistent value when the simulation is run on different angular velocity. Based on Figure 7 and Figure 8, the CFD simulation results follows the experimental result closely. For 6X4E propeller, the Ct value is overestimated at higher advance ratio as shown in Figure 7. Meanwhile, the C_Q value for 6X4E is overestimated at all advance ratios. The average percentage error for C_T and C_Q at different angular velocity is 11.50% and 27.49% respectively. For 9X6E propeller, both C_T and C_Q simulation result matches the experimental result closely and the C_Q value is overestimated at lower and higher advance ratio. The average percentage error for C_T and C_q at different angular velocity is 8.40% and 16.7% respectively. For propeller efficiency, N_P, the CFD simulation results follows the experimental value closely with slight overestimation for both 6X4E and 9X6E propeller. The average percentage error for N_P at different angular velocity is 13.59% and 11.52% for 6X4E and 9X6E respectively.

There are different reasons that contribute to the error of the CFD simulation. The main source of error for the CFD simulation is the CAD modelling of the propeller. Firstly, the information on the aerofoil of the propeller blade is limited. The aerofoil of the propeller blade is only described as low Reynolds number Eppler E63 aerofoil blended with a Clark-Y similar aerofoil at the tip of the propeller blade. Besides, the limitation of measuring tools used to measure the dimension of the propellers also contribute to the error of the simulation. The top and side view of the propeller is sketched and a digital vernier calliper is used to measure the width at different distance of the propeller blade. The limitation of the vernier calliper to measure the distance accurately will contribute to the error. Besides, the blade angle of twist cannot be measured without the specific tools such as 3D scanner. Information on the propeller blade chord and twist distribution of 9X6E propeller are obtained from UIUC propeller database and combined with the dimension measured using vernier calliper, therefore the error of CFD simulation is lower. Meanwhile there is no information on the chord and

twist distribution of 6X4E propeller blade. Hence, the error of the CFD simulation on 6x4E propeller is higher than that of 9X6E propeller.
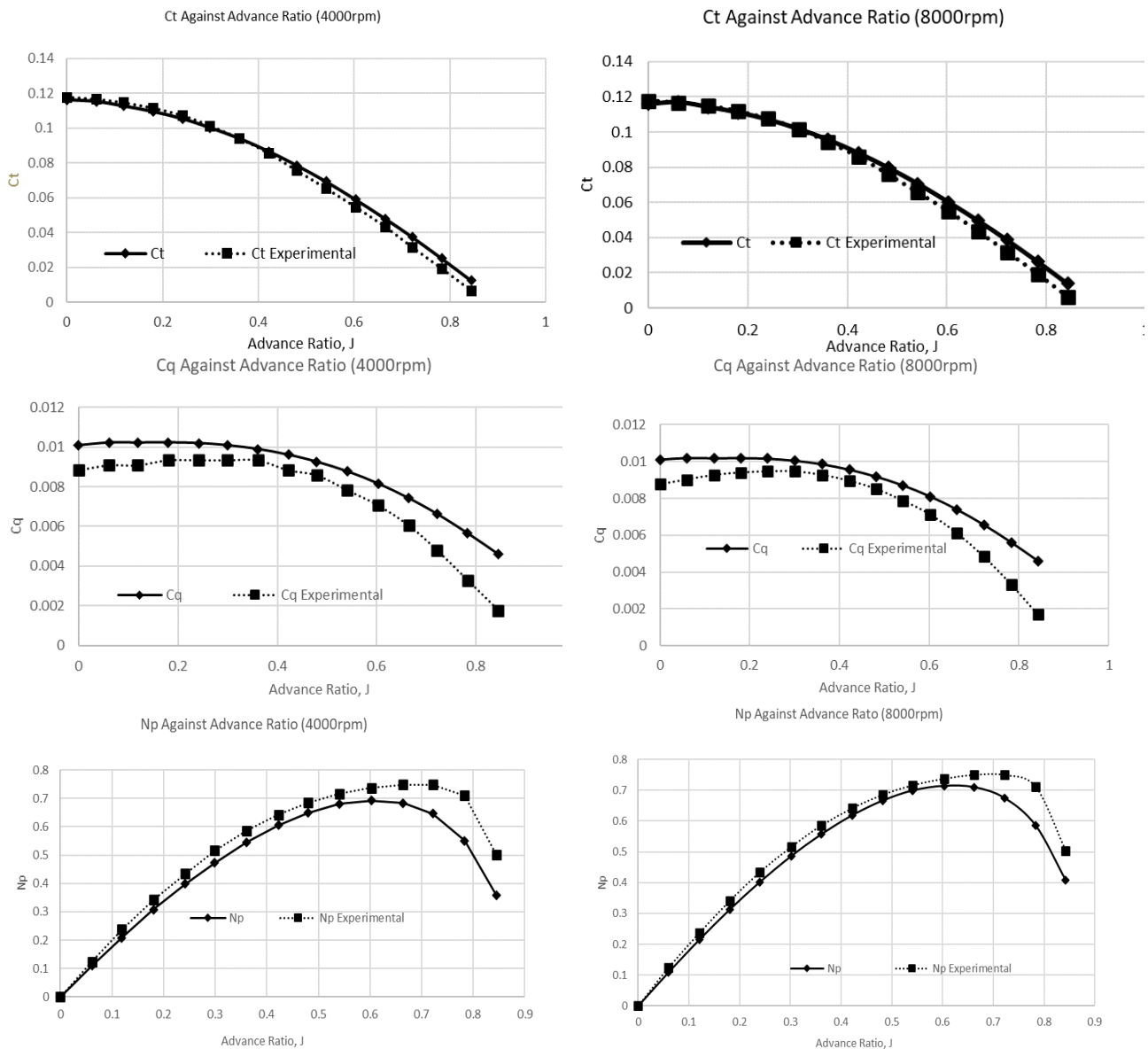

Fig. 7. C_T, C_Q and N_p against Advance Ratio for 6x4E at 4000rpm and 8000rpm
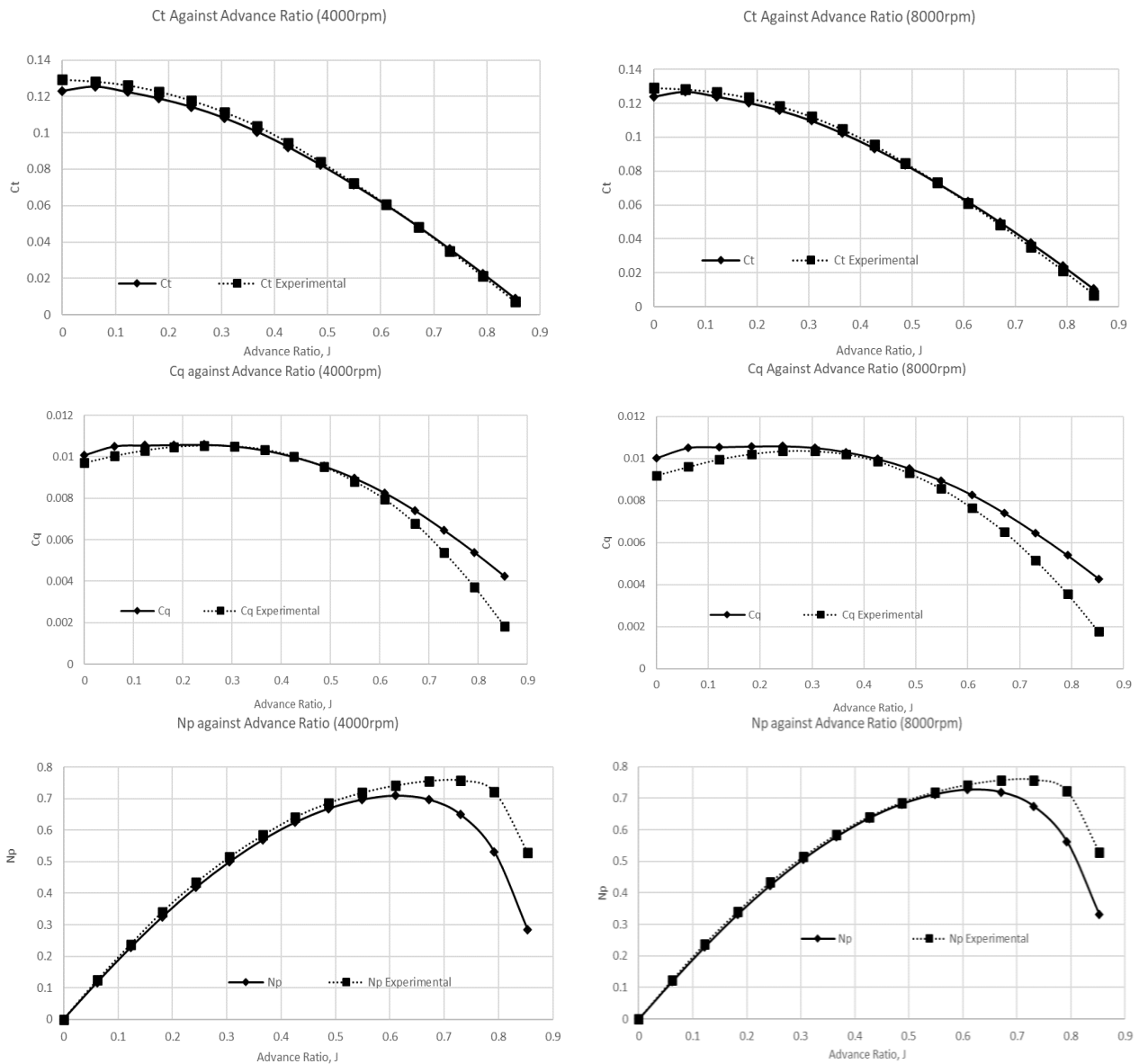
Fig. 8. C_T, C_Q and N_p against Advance Ratio for 9X6E at 4000rpm and 8000rpm

3.2 Propeller Performance at Different Propeller Disc Angle

The thrust and torque coefficient for both 6X4E and 9X6E APC propeller at varying advance ratio and propeller disc angle is obtained via CFD simulation. The simulation is conducted at angular velocity of 4000rpm, propeller disc angle of 30°, 60° and 90° and advance ratio ranging from 0 to 0.88. 4000rpm is chosen as the model and analysis due the less error yielded during 0 angle at different advance ratio. The results for both 6X4E and 9X6E in figures below show that the thrust coefficient increases with the increasing propeller disc angle at the same advance ratio. For propeller disc angle of 0°, 30° and 60°, the thrust coefficient decreases as the advance ratio increases. Meanwhile, the thrust coefficient at 90° propeller disc angle increases with the increasing advance ratio. It is also evident that the difference of thrust coefficient at different propeller angle is minimal at advance ratio < 0.3. The results obtained from the CFD simulation matches with the results obtained by Serrano *et al.,* [1] where the thrust coefficient decreases with increasing advance ratio at propeller disc angle ≤ 60° and increases with increasing advance ratio at propeller disc angle ≥ 70°.

As for torque coefficient, the CFD simulation result shows that the torque coefficient increases with increasing propeller disc angle at the same advance ratio except for thrust coefficient at α = 60° smaller than that of 30°. For propeller disc angle of 0°, 30° and 60°, the torque coefficient decreases as the advance ratio increases. Meanwhile, the torque coefficient at 90° propeller disc angle increases with the increasing advance ratio. The torque coefficient at advance ratio ≤ 0.3 also shows overlap and minimal difference indicating that the propeller disc angle only affects the torque coefficient slightly at low advance ratio.

According to Figure 9, Figure 10 and Figure 11, the propeller efficiency increases with increasing propeller disc angle of attack at the constant advance ratio. For 0° propeller disc angle, the propeller efficiency increases with increasing advance ratio until the maximum efficiency around advance ratio of 0.6 and then decreases with the increasing advance ratio. For propeller disc angle > 0°, the propeller efficiency increases with increasing advance ratio. At advance ratio ≤ 0.3, the propeller efficiency at different propeller disc angle overlaps and there ARE only small differences of the efficiency. These CFD simulation results matches the wind tunnel results obtained by Serrano *et al.,* [1] closely.
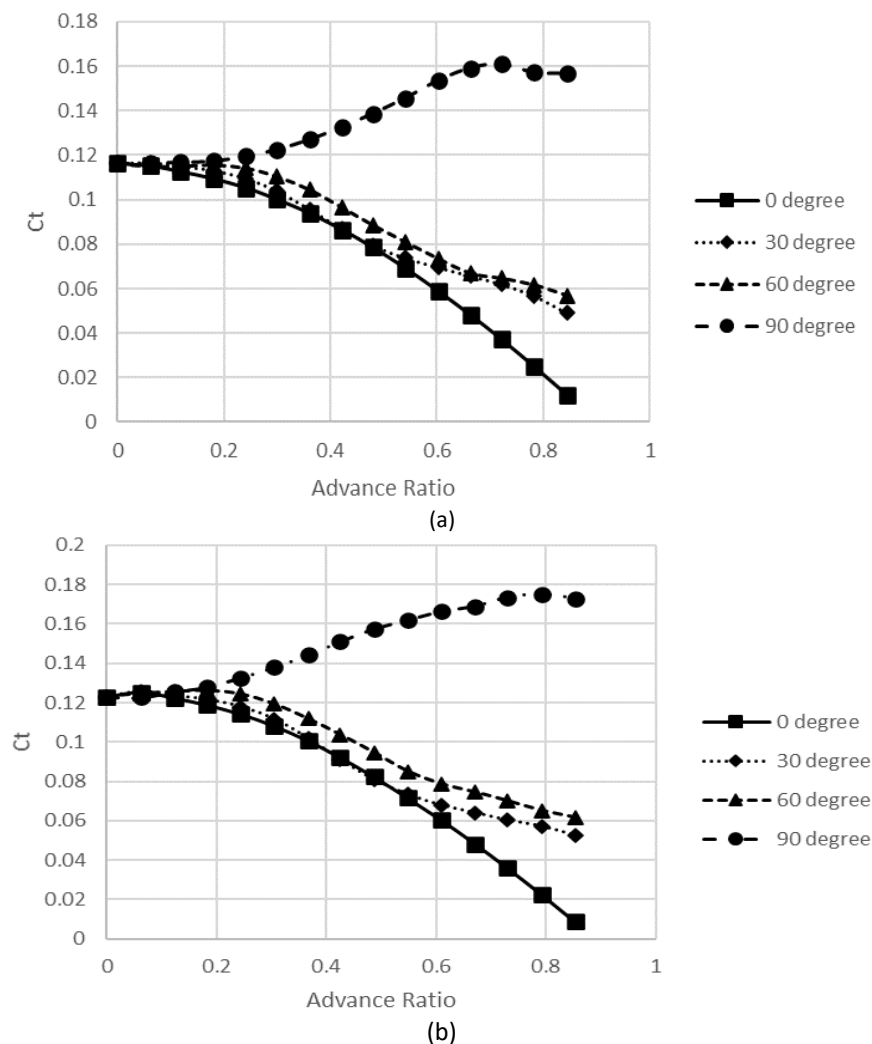

Fig. 9. Coefficient of thrust, C_T against advance ratio at different angle for (a) 6X4E propeller (b) 9x6E
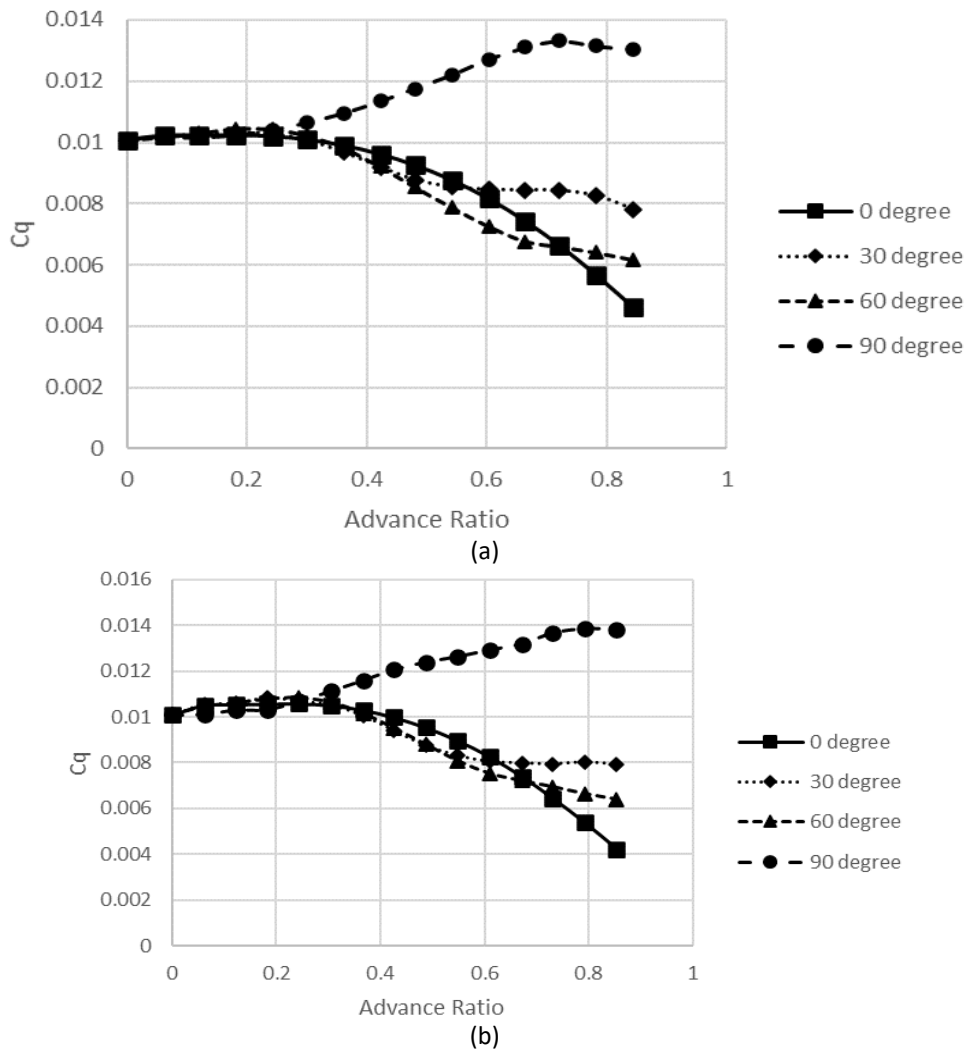
Fig. 10. Coefficient of torque, C_Q against advance ratio for (a) 6X4E propeller (b) 9x6E
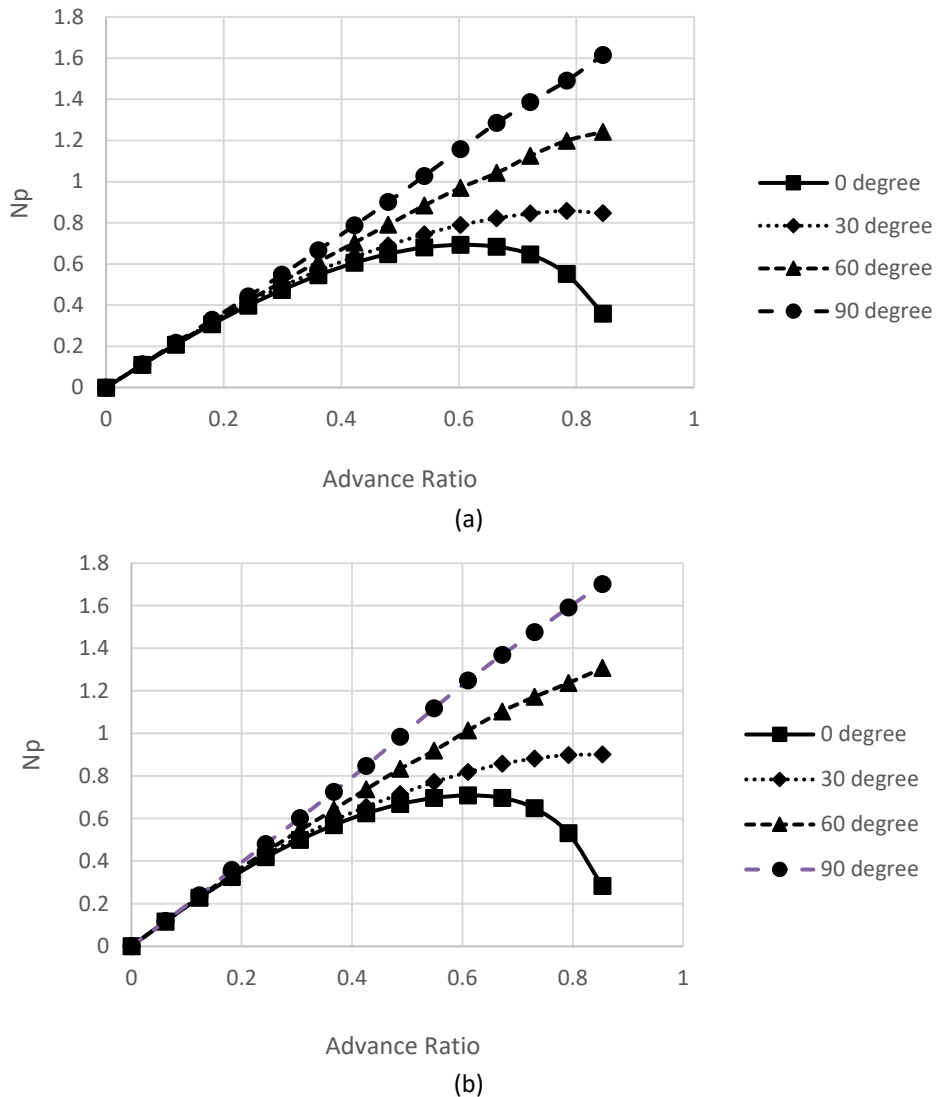
(a)

(b)

Fig. 11. Efficiency, N_P against advance ratio for (a) 6X4E propeller (b) 9x6E

4. Conclusions

Two CFD analysis was conducted, one is the CFD simulation on 9x6E and 6x4E APC propellers conducted using ANSYS FLUENT at different advance ratio from 0 to 0.88 and different rpm at 4000rpm and 8000rpm. The percentage error of the CFD simulation on 6X4E propeller is higher than that of 9X6E propeller. Second, the CFD simulation on 9X6E and 6X4E APC propellers conducted at advance ratio ranging from 0 to 0.8 and propeller disc angle of 0°, 30°, 60°, and 90° at 4000rpm. The C_T, C_Q and N_P against advance ratio curves generated from CFD simulation followed the trend of the wind tunnel testing data conducted by Serrano *et al.,* [1].

Multiple reference frame method is used to simulate the rotating of the propeller in the flowing airstream. Tetrahedral mesh is constructed, and mesh convergence test is conducted to minimize the discretization error. By comparing the simulation results from different turbulence model, SST k-ω model is found to provide more result with higher accuracy compared to standard k-ε model, Spalart-Allmaras (S-A) model, and standard k-ω model.

The CFD analysis shows that the turbulence model and the mesh used are acceptable in comparison to the wind tunnel test for thrust performance estimation but improvement on meshing configuration can be done for torque performance estimation. The error produce for thrust

estimation is lower than 12% for both 6x4E and 9x6E propellers. The error for torque and efficiency estimation is between 15-30% and 12% respectively.

Acknowledgement

References

[1]   Serrano, David, Max Ren, Ahmed Jawad Qureshi, and Sina Ghaemi. "Effect of disk angle-of-attack on aerodynamic performance of small propellers." *Aerospace Science and Technology* 92 (2019): 901-914. https://doi.org/10.1016/j.ast.2019.07.022

[2]   Seeni, Aravind, Parvathy Rajendran, and Hussin Mamat. "A CFD Mesh Independent Solution Technique for Low Reynolds Number Propeller." *CFD Letters* 11, no. 10 (2019): 15-30.

[3]   Cable, Matthew. "An evaluation of turbulence models for the numerical study of forced and natural convective flow in Atria." *PhD diss., Queen's University*, 2009.

[4]   Zienkiewicz, O. C., R. L. Taylor, and P. Nithiarasu. "Chapter 8-Turbulent flows." *The Finite Element Method for Fluid Dynamics*, 7th edn. Butterworth-Heinemann (2014): 283-308. https://doi.org/10.1016/B978-1-85617-635-4.00008-X

[5]   Kutty, Hairuniza Ahmed, and Parvathy Rajendran. "3D CFD simulation and experimental validation of small APC slow flyer propeller blade." *Aerospace* 4, no. 1 (2017): 10. https://doi.org/10.3390/aerospace4010010

[6]   Duan, Xiaoxia, Xin Feng, Chao Yang, and Zaisha Mao. "CFD modeling of turbulent reacting flow in a semi-batch stirred-tank reactor." *Chinese Journal of Chemical Engineering* 26, no. 4 (2018): 675-683. https://doi.org/10.1016/j.cjche.2017.05.014

[7]   Menter, Florian R. "Two-equation eddy-viscosity turbulence models for engineering applications." *AIAA Journal* 32, no. 8 (1994): 1598-1605. https://doi.org/10.2514/3.12149

[8]   Brandt, John, and Michael Selig. "Propeller performance data at low reynolds numbers." In *49th AIAA Aerospace Sciences Meeting including the New Horizons Forum and Aerospace Exposition*, p. 1255. 2011. https://doi.org/10.2514/6.2011-1255

[9]   Silvestre, Miguel, João Morgado, Pedro Alves, Pedro Santos, Pedro Gamboa, and José Páscoa. "Low Reynolds Number Propeller Performance Testing." *Recent Advances in Mechanical Engineering* (2014).

[10]   Wendt, John F., ed. *Computational fluid dynamics: an introduction*. Springer Science & Business Media, 2008.

[11]   Wei, Xinli, Jie Ren, and Xiangrui Meng. "Simulation and Experiment Study of Flow Field and Dynamic Performance in Stirred Reactor." In *Challenges of Power Engineering and Environment*, pp. 1408-1413. Springer, Berlin, Heidelberg, 2007. https://doi.org/10.1007/978-3-540-76694-0_265

[12]   Yilmaz, Serdar, Duygu Erdem, and Mehmet S. Kavsaoglu. "Performance of a ducted propeller designed for UAV applications at zero angle of attack flight: An experimental study." *Aerospace Science and Technology* 45 (2015): 376-386. https://doi.org/10.1016/j.ast.2015.06.005

[13]   Ab Wahid, M., A. N. Asmi, N. Othman, M. I. Ardani, MZ Md Zain, and S. Mansor. "The effect of different motor constants to an commercial propeller." In *IOP Conference Series: Materials Science and Engineering*, vol. 884, no. 1, p. 012096. IOP Publishing, 2020. https://doi.org/10.1088/1757-899X/884/1/012096

[14]   Loureiro, Eric Vargas, Nicolas Lima Oliveira, Patricia Habib Hallak, Flávia de Souza Bastos, Lucas Machado Rocha, Rafael Grande Pancini Delmonte, and Afonso Celso de Castro Lemonge. "Evaluation of low fidelity and CFD methods for the aerodynamic performance of a small propeller." *Aerospace Science and Technology* 108 (2021): 106402. https://doi.org/10.1016/j.ast.2020.106402

[15]   Mohamed, Wan Mazlina Wan, Nirresh Prabu Ravindran, and Parvathy Rajendran. "A CFD Simulation on the Performance of Slotted Propeller Design for Various Airfoil Configurations." *CFD Letters* 13, no. 3 (2021): 43-57. https://doi.org/10.37934/cfdl.13.3.4357

[16]   Brandt, John B, Robert W Deters, and Gavin K Ananda. "UIUC Propeller Database - Volume 2." UIUC Propeller Data Site. UIUC Applied Aerodynamics Group, May 27, 2015.